

Optimal TDI2.0 of sensitive curve for main space GW detector

Yu Tian, Zhi-Xiang Li¹

¹*School of Fundamental Physics and Mathematical Sciences,
Hangzhou Institute for Advanced Study, UCAS, Hangzhou 310024, China*
(Dated: April 28, 2023)

Time-delay interferometry (TDI) is a crucial technology for space-based gravitational wave detectors. Previous studies have identified the optimal TDI configuration for the first-generation. In this research, we used an Algebraic approach theory to describe the TDI space and employed a method to maximize the signal-to-noise ratio (SNR) to derive the optimal TDI combination for the second-generation. When this combination is used in the sensitivity curve, we observed enhancements of up to 1.91 times in the low-frequency domain and 2 to 3.5 times in the high-frequency domain compared to the Michelson combination. Furthermore, changes in the detector index significantly affect the optimization effect. We also present detection scenarios for several low-frequency gravitational wave sources. Compared to the first-generation TDI optimization, the SNR value for verification double white dwarfs (DWD) and the detection rate for DWD increase by 16.5%.

I. INTRODUCTION

The discovery of gravitational waves (GW) has greatly advanced the field of gravitational wave astronomy [1, 2]. It has led to the emergence of a new astronomy era that involves multi-band detection [3–7], multi-messenger detection, and various gravitational wave detectors. Furthermore, it has provided a new way to test theoretical models in various fields. Currently, gravitational wave detections cover the main frequency band above 1Hz, which includes pulsars and supernovae. Lower frequency gravitational waves in the range of $10^{-4}Hz - 1Hz$ are detected using methods such as Extreme Mass Ratio Inspirals (EMRI) and compact binaries [8]. Meanwhile, supermassive black holes (SMBH) emit gravitational waves in the frequency band of $10^{-9}Hz - 10^{-2}Hz$ [9]. Gravitational wave detectors that operate in this frequency band include LISA [10], Taiji [11], and Tianqin [12]. Based on theoretical models of main GW sources, we can search for the optimal data processing methods for specific scientific objectives and detect different wave sources within the existing conditions to achieve maximum scientific satisfaction.

Ground-based wave detectors such as LIGO and Virgo can suppress laser frequency noise to a very low level due to the minimal change of arm length. However, if the Michelson interference is placed in space to detect low-frequency sources, the ground gravity gradient noise level is too high to achieve the same effect [13]. In space gravitational wave detectors, gravitational waves are detected through monitoring interference signals. The optical path between adjacent satellites constantly changes over time, leading to laser channel noise of an unacceptable magnitude [14]. To suppress laser frequency noise, Time Delay Interferometry (TDI) is the main arithmetic [15–19]. Sensitivity curves are a useful tool to show the influence of different TDI configurations. The equal-arm configuration TDI1.0 [20] has been widely used in space gravitational wave detectors. However, the unequal-arm configuration TDI2.0 [21] is more suitable for real de-

tection situations due to the movement of the satellites. This configuration can effectively reduce the impact of satellite drift and have a sufficiently small residual laser phase noise to extract gravitational waves. TDI X channel can suppress laser frequency noise by up to eight orders of magnitude. Compared to the X configuration, the existing first-generation optimal TDI channel combination, A, E, T [22, 23], can be improved by $\sqrt{2}$ in low frequency and $\sqrt{3}$ in high frequency. Currently, K. Rajesh Nayak has generalized the corresponding TDI form for the known direction of the wave source [24, 25].

In this paper, we have obtained the optimal sensitivity by optimum weighting of second-generation Time Delay Interferometry (TDI) configurations, which results in an optimal signal-to-noise ratio (SNR) for detecting primary types of target gravitational wave sources. Compared to the TDI X channel, the second-generation optimal configuration can improve the sensitive curve by up to 1.91 times under the low-frequency approximation and get 2 times even up to 3.5 times in the high-frequency approximation at certain frequency points. This improvement can effectively enhance the source detection rate and SNR. Moreover, using the code published by Ollie Burke and Andrea Antonelli, our proposed channel can improve the parameter estimation accuracy by up to 2 times in case of source confusion with deviation accumulation and by up to 10 times in the case of global fit.

The paper is organized as follows. In Section II, we briefly introduce the basic process of the first-generation optimal TDI and explain the idea and development process behind the second-generation optimal TDI. In Section III, we obtain the PSD formula and sensitivity curve of the second-generation optimal TDI and compare it with other TDI configurations. In Section IV, we evaluate the SNR values and detection rates of the target wave source based on the optimal TDI configuration. In Section V, we apply parameter estimation.

II. TDI1.0 AND TDI2.0 CONFIGURATION OF OPTIMAL SNR

In this section, we provide a brief overview of TDI, as necessary for the analysis presented in Fig. 1. For space-based gravitational wave detectors, the Michelson interferometer is typically used on three satellites in orbit, labeled SC_i . The corresponding optical paths are denoted by $L1, L2$, and $L3$ ($L1', L2', L3'$) in counterclockwise (clockwise) order, and yield six basic data streams denoted by U_i and V_i . The data is recorded by measuring the Doppler shift phase, including both noise and gravitational wave signals. In this work, we consider only the simplest case and ignore all other noises except shot noise and acceleration noise. The frequency fluctuation of the data stream is given by [26].

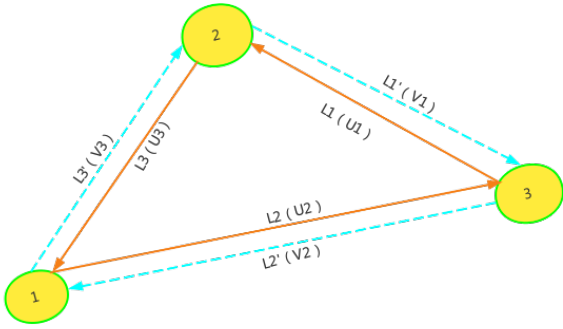


FIG. 1: Optical path configuration of space gravitational wave detector

$$C_i(t) = \frac{\Delta V_i(t)}{V_0(t)} \quad (1)$$

where $\Delta V_i(t)$ is frequency fluctuation ($V(t)$ is reference frequency) of the laser on SC_i , t is gravitational wave travel time between adjacent SC.

Laser frequency noise is a major source of interference that affects the accuracy of gravitational wave detection. To mitigate this effect, the main technology used is time delay interference (TDI), which involves time-delaying the data streams and recombining them linearly. This technique assumes that the data streams between the two optical benches (OBs) in each SC are equal, and introduces time delay interference data streams. The time delay interference operator $D_j C_i(t)$ is defined as $C_i(t - \frac{L_j}{c})$ [27], and the time delay interference data stream is expressed mathematically as follows:

$$\begin{aligned} U_i &= D_{(i+1)} C_{(i+2)} - C_i \\ V_i &= C_i - D_{(i+2)} C_{(i+1)} \end{aligned} \quad (2)$$

Combine all the data streams, ideally eliminating all laser frequency noise, and get

$$\sum_{i=1}^3 p_i V^i + p_i' U^i = 0 \quad (3)$$

where p_i and p_i' is coefficient of time delay interference operator.

The current several major configurations of coefficient of q_i and q_i' are express in [19][23] [28]. So let's list the needed-configuration coefficients

TDIX₁

$$\begin{aligned} P_1 &= (\mathcal{D}_{2'2} - 1), P_2 = 0, P_3 = (\mathcal{D}_{2'} - \mathcal{D}_{33'2'}) \\ P_{1'} &= (1 - \mathcal{D}_{33'}) P_{2'} = (\mathcal{D}_{2'23} - \mathcal{D}_3) P_{3'} = 0 \end{aligned}$$

TDIX₂

$$\begin{aligned} P_1 &= -(1 - \mathcal{D}_{2'2} - \mathcal{D}_{2'233'} + \mathcal{D}_{33'2'2'2}), P_2 = 0 \\ P_3 &= (1 - \mathcal{D}_{33'} - \mathcal{D}_{33'2'2} + \mathcal{D}_{2'233'33'}) \mathcal{D}_{2'} \\ P_{1'} &= (1 - \mathcal{D}_{33'} - \mathcal{D}_{33'2'2} + \mathcal{D}_{2'233'33'}) \\ P_{2'} &= -(1 - \mathcal{D}_{2'2} - \mathcal{D}_{2'233'} + \mathcal{D}_{33'2'2'2}), P_{3'} = 0 \end{aligned} \quad (4)$$

TDI Sagnac basis α_2

$$\begin{aligned} P_1 &= (1 - \mathcal{D}_{2'1'3'}), P_{1'} = -(1 - \mathcal{D}_{312}), \\ P_2 &= (1 - \mathcal{D}_{2'1'3'}) \mathcal{D}_3, P_{2'} = -(1 - \mathcal{D}_{312}) \mathcal{D}_{2'1'}, \\ P_3 &= (1 - \mathcal{D}_{2'1'3'}) \mathcal{D}_{31}, P_{3'} = -(1 - \mathcal{D}_{312}) \mathcal{D}_{2'} \end{aligned}$$

get β_2 and γ_2 though rotation ($1 \rightarrow 2 \rightarrow 3 \rightarrow 1$)

The signal-to-noise ratio (SNR) is a crucial parameter for assessing gravitational wave sources. The first-generation TDI was designed to address the equal-arm case, while the second-generation TDI is capable of handling situations where L_i and L_i' differ not only in value but also in their time dependence. It is clear that the first-generation TDI is insufficient in eliminating laser frequency noise of orders higher than speed. This has an impact on the SNRs that are considered significant in contributing to the results.

The purpose of this section is to derive the optimal sensitivity by optimum weighting of second-generation Time Delay Interferometry (TDI) configurations under the following assumptions: 1) Noise independence; 2) Other second-generation TDI configurations can be obtained by linearly combining the generators $\alpha_2, \beta_2, \gamma_2, X_2$ in Eq.(4). Tinto has shown that it is possible to derive a family of ζ -like combinations [27][29]; 3) $L1=L2=L3$, so $D=D_i$ and $D^2 = D_{ij}$. The generators of ζ -like combinations TDI algebraic space are four. TDI algebraic space can be obtain

$$TDI(f) = \sum \lambda_i(f, a) X_i \quad (5)$$

where $\lambda_i(f, a)$ are arbitrary complex functions of the Fourier frequency f , a is Characteristic parameters of gravitational waves, X_i are TDI space generator.

SNR can be get by [27]

$$SNR^2 = \int \frac{|\sum \lambda_i(f, a) X_i^s|^2}{|\sum \lambda_i(f, a) X_i^n|^2} \quad (6)$$

where subscripts s and n refer to the signal and the noise parts of TDI space generator. After a series of algebraic processes such as differentiation and derivation in [27][30], we can get

$$\text{SNR}_{\text{opt}}^2 = \int \mathbf{x}_i^{(s)*} (\mathbf{C}^{-1})_{ij} \mathbf{x}_j^{(s)} df \quad (7)$$

The correlation matrix in TDI generator space is given by $C = \langle X_i^n, X_j^n \rangle$, which is Hermitian and non-singular. Currently, the optimal TDI1.0 configuration, which consists of A, E, and T, has been obtained. By combining these three configurations, the first-generation optimal TDI can increase the SNR value by $\sqrt{2}$ times in the low-frequency range and $\sqrt{3}$ times in the high-frequency range [25].

Based on the previous assumptions, where the matrix C is 4×4 , The noise correlation matrix C is uniquely identified by two real functions, S_a and S_{ab} . So the matrix C can be expressed by

$$C = \begin{pmatrix} S_a & S_{ab} & S_{ab} & S_{ab} \\ S_{ab} & S_a & S_{ab} & S_{ab} \\ S_{ab} & S_{ab} & S_a & S_{ab} \\ S_{ab} & S_{ab} & S_{ab} & S_a \end{pmatrix} \quad (8)$$

Based on the previous assumptions, the optimal signal-to-noise ratio can be converted to the sum of the 'converted' signal-to-noise ratio of the four interference combinations. By using Mathematica code, it is easy to obtain the four eigenvalue matrices C.

$$(S_a - S_{ab}, S_a - S_{ab}, S_a - S_{ab}, S_a + 3S_{ab}) \quad (9)$$

After orthogonalization of all the eigenvectors, the first three eigenvectors correspond to the same eigenvalue, while the fourth eigenvector corresponds to an eigenvalue orthogonal to them. we get

$$\begin{aligned} A_1 &= \frac{1}{\sqrt{2}}(-\alpha_2 + X_2) \\ A_2 &= \frac{1}{\sqrt{2}}(-\alpha_2 + \gamma_2) \\ A_3 &= \frac{1}{\sqrt{2}}(-\alpha_2 + \beta_2) \\ B &= \frac{1}{2}(\alpha_2 + \beta_2 + \gamma_2 + X_2) \end{aligned} \quad (10)$$

In this section, we obtain the second-generation optimal TDI combination to maximize the SNR value. Although its form is somewhat similar to the first-generation optimal TDI, it has some more interesting properties that will be studied in the following sections.

III. SENSITIVITY CURVE

A. PSD

To achieve optimal signal-to-noise ratio for the detection of gravitational wave sources, a simple toy model is used that considers the addition of proof mass and shot noise in the noise power spectral density [10–12]. The resulting linear combination of total residual power spectral densities of proof mass and shot noise can be expressed as [28, 31].

$$\begin{aligned} \text{PSD}(u) &= S_{\text{TDI}^a}(u) + S_{\text{TDI}^{\text{shot}}}(u) \\ &= C_1 [\tilde{P}_i(u)] n_1(u) + 4C_2 [\tilde{P}_i(u)] n_2(u), \end{aligned} \quad (11)$$

where C_1 and C_2

$$\begin{aligned} C_1 [\tilde{P}_i(u)] &= \sum_{i=1}^3 \text{Re} \left[\left| \tilde{P}_i \right|^2 + \left| \tilde{P}_{i'} \right|^2 \right], \\ C_2 [\tilde{P}_i(u)] &= \sum_{i=1}^3 \text{Re} \left[\tilde{P}_i \tilde{P}_{(i+1)'}^* \right], \end{aligned} \quad (12)$$

$$n_1(u) = 2S_{\text{pf}} + S_{\text{opt}}, n_2(u) = S_{\text{pf}} \cos u, \quad (13)$$

with $u = (2\pi f L/c)$. $S_{\text{pf}} = \frac{s_a^2}{(2\pi f c)^2}$ and $S_{\text{shot}} = \frac{(2\pi f)^2 s_x^2}{c^2}$, where s_a and s_x are amplitude spectral densities (ASDs) of proof mass acceleration and shot noises, respectively. By use In Sec. II TDI coefficient, the PSD are obtained for $L_1 = L_2 = L_3 = L$ in following list:

$$\begin{aligned} \text{SX1PSD}[f] &= (16(3 + \cos[4f(L/c)\pi]) \sin[2fL\pi]^2) S_a \\ &\quad + S_x 16 \sin[2f(L/c)\pi]^2 \end{aligned} \quad (14)$$

$$\begin{aligned} \text{X2PSD}(f) &= 256 S_a \cos[2f(L/c)\pi]^2 (3 + \cos[4f(L/c)\pi]) \\ &\quad \sin[2f(L/c)\pi]^4 + 64 S_x \sin[2f(L/c)\pi]^2 \\ &\quad \sin[4f(L/c)\pi]^2. \end{aligned} \quad (15)$$

$$\begin{aligned} \text{SA1PSD}(f) &= \text{SA2PSD}(f) = \text{SA3PSD}(f) \\ &= 16 S_a \sin^4(\pi f(L/c)) (344 \cos(2\pi f(L/c)) \\ &\quad + 244 \cos(4\pi f(L/c)) + 136 \cos(6\pi f(L/c)) \\ &\quad + 56 \cos(8\pi f(L/c)) + 16 \cos(10\pi f(L/c)) \\ &\quad + 4 \cos(12\pi f(L/c)) + 195) \\ &\quad + S_x (4 \cos(2\pi f(L/c)) - 2(3 \cos(4\pi f(L/c)) \\ &\quad + 4 \cos(6\pi f(L/c)) + 4 \cos(8\pi f(L/c)) \\ &\quad + \cos(10\pi f(L/c)) - 3 \cos(12\pi f(L/c)) - 7)) \end{aligned} \quad (16)$$

$$\begin{aligned}
\text{SBPSD}(f) = & 8 \text{Sa} \sin^4(\pi f(L/c)) (280 \cos(2\pi f(L/c)) \\
& + 188 \cos(4\pi f(L/c)) + 92 \cos(6\pi f(L/c)) \\
& + 28 \cos(8\pi f(L/c)) + 4 \cos(10\pi f(L/c)) \\
& + 163) + \text{Sx} (10 \cos(2\pi f(L/c)) - 2 \cos(4\pi f(L/c)) \\
& - 11 \cos(6\pi f(L/c)) - 12 \cos(8\pi f(L/c)) \\
& - 3 \cos(10\pi f(L/c)) + 2 \cos(12\pi f(L/c)) \\
& + \cos(14\pi f(L/c)) + 15)
\end{aligned} \tag{17}$$

Reference some published literature parameters for Taiji, LISA, tianqin GW detector in Table. I, The noise comparison diagram is shown in Fig. 2, Fig. 3, Fig. 4.

TABLE I: Parameters for GW detectors

Detector	L (m)	sa ($\text{m/s}^2/\sqrt{\text{Hz}}$)	sx ($\text{m}/\sqrt{\text{Hz}}$)
Taiji	$30 \cdot 10^8$	$3 \cdot 10^{-15}$	$8 \cdot 10^{-12}$
LISA	$25 \cdot 10^8$	$3 \cdot 10^{-15}$	$15 \cdot 10^{-12}$
Tianqin	$1.7 \cdot 10^8$	$1 \cdot 10^{-15}$	$1 \cdot 10^{-12}$

where sa is Acceleration noise, sx is shot noise

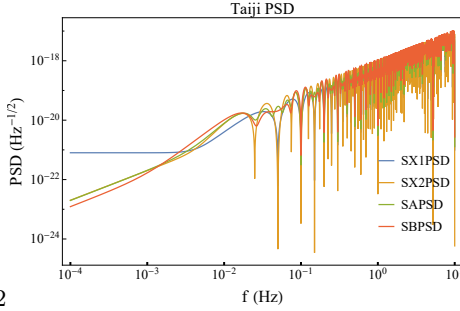


FIG. 2: The comparison of taiji noise power spectral density (PSD) mainly includes TDI1.0X configuration, TDI2.0X configuration, TDI2.0A configuration and TDI2.0B configuration.

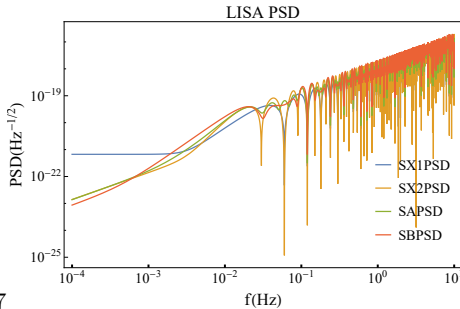


FIG. 3: The comparison of LISA noise power spectral density (PSD) mainly includes TDI1.0X configuration, TDI2.0X configuration, TDI2.0A configuration and TDI2.0B configuration.

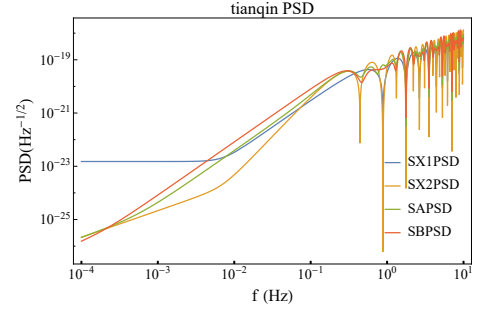


FIG. 4: The comparison of tianqin noise power spectral density (PSD) mainly includes TDI1.0X configuration, TDI2.0X configuration, TDI2.0A configuration and TDI2.0B configuration.

B. The GW All-sky averaged response function

In this section, the performance of different second-generation TDI configurations is investigated under the assumption of an average spherical polarization of gravitational waves and a simple noise model. To this end, a published response function [28, 31] is used to illustrate the differences between the configurations.

As to common TDI combination reads

$$\begin{aligned}
R(u) = & \frac{2}{4} C_1 [\tilde{P}_i(u)] \times f_1(u) \\
& + C_2 [\tilde{P}_i(u)] \times f_2(u) \\
& + \frac{3}{4} C_3 [\tilde{P}_i(u)] \times f_3(u) \\
& - \frac{3}{4} C_4 [\tilde{P}_i(u)] \times f_4(u) \\
& + \frac{1}{4} C_5 [\tilde{P}_i(u)] \times f_5(u)
\end{aligned} \tag{18}$$

$$\begin{aligned}
f_1(u) &= \frac{4}{3} - \frac{2}{u^2} + \frac{\sin 2u}{u^3} \\
f_2(u) &= \frac{-u \cos u + \sin u}{u^3} - \frac{\cos u}{3} \\
f_3(u) &= \log \frac{4}{3} - \frac{5}{18} + \frac{-5 \sin u + 8 \sin 2u - 3 \sin 3u}{8u} \\
&\quad - \frac{1}{3} \left(\frac{4 + 9 \cos u + 12 \cos 2u + \cos 3u}{8u^2} \right) \\
&\quad + \frac{1}{3} \left(\frac{-5 \sin u + 8 \sin 2u + 5 \sin 3u}{8u^3} \right) + \text{Ci}3u - 2\text{Ci}2u + \text{Ci}u \\
f_4(u) &= \frac{-5 \cos u + 8 \cos 2u - 3 \cos 3u}{8u} - \text{Si}3u - \text{Si}u + 2\text{Si}2u \\
&\quad + \frac{1}{3} \left(\frac{9 \sin u + 12 \sin 2u + \sin 3u}{8u^2} - \frac{8 + 5 \cos u}{8u^3} \right) \\
&\quad + \frac{1}{3} \left(-\frac{8 \cos 2u - 5 \cos 3u}{8u^3} \right) \\
f_5(u) &= -\log 4 + \frac{7}{6} + \frac{11 \sin u - 4 \sin 2u}{4u} \\
&\quad - \frac{10 + 5 \cos u - 2 \cos 2u}{4u^2} \\
&\quad + \frac{5 \sin u + 4 \sin 2u}{4u^3} + 2(\text{Ci}2u - \text{Ci}u)
\end{aligned} \tag{19}$$

$$\begin{aligned}
C_1 &= \sum_{i=1}^3 \left[\left| \tilde{P}_i \right|^2 + \left| \tilde{P}_{i'} \right|^2 \right] \\
C_2 &= 2 \sum_{i=1}^3 \text{Re} \left[\tilde{P}_i \tilde{P}_{(i+1)'}^* \right] \\
C_3 &= 2 \sum_{i=1}^3 \text{Re} \left[\left(\tilde{P}_i \tilde{P}_{i+1}^* + \tilde{P}_{i'} \tilde{P}_{(i-1)'}^* \right) e^{iu} \right] \\
C_4 &= 2 \sum_{i=1}^3 \text{Im} \left[\left(\tilde{P}_i \tilde{P}_{i+1}^* + \tilde{P}_{i'} \tilde{P}_{(i-1)'}^* \right) e^{iu} \right] \\
C_5 &= 2 \sum_{i=1}^3 \text{Re} \left[\tilde{P}_i \tilde{P}_{i'}^* + \tilde{P}_i \tilde{P}_{(i-1)'}^* \right]
\end{aligned} \tag{20}$$

For the TDI2.0 A and B combinations, by substitute Eq.10 into Eq.18, Detailed calculate results are obtained for needed configuration, and low frequency limit and high frequency limit results can be obtained for similar way. Fig.5, Fig.6, Fig.7 are shown in following list at low frequency limit.

C. sensitive and Optimization comparison

The calculation formula of SNR and the construction method of sensitivity curve are briefly introduced. The definition of SNR for all sky average is quoted[32]:

$$SNR^2 = T \int \frac{H^2}{PSD(u)/R(u)} df \tag{21}$$

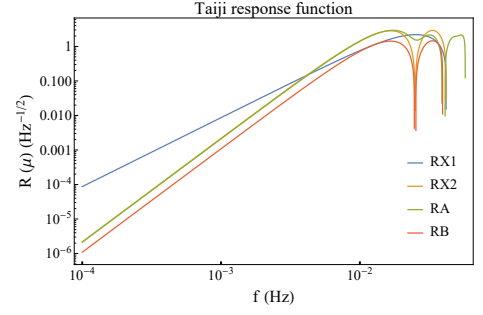


FIG. 5: The comparison of Taiji GW averaged response function mainly includes TDI1.0X configuration, TDI2.0X configuration, TDI2.0A configuration and TDI2.0B configuration.

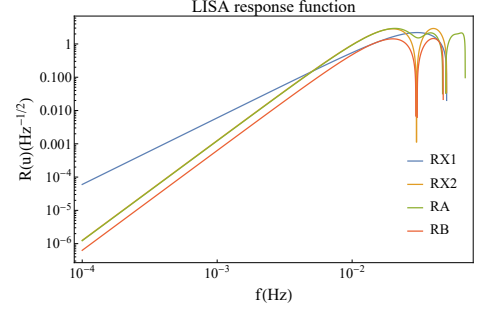


FIG. 6: The comparison of LISA GW averaged response function mainly includes TDI1.0X configuration, TDI2.0X configuration, TDI2.0A configuration and TDI2.0B configuration.

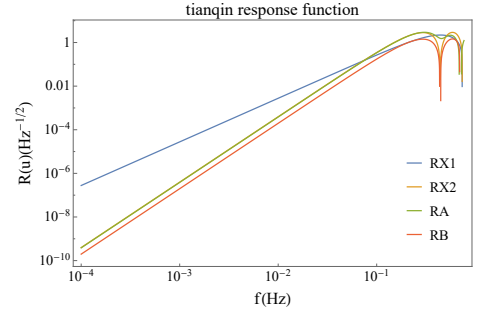


FIG. 7: The comparison of Tianqin GW averaged response function mainly includes TDI1.0X configuration, TDI2.0X configuration, TDI2.0A configuration and TDI2.0B configuration.

where H is GW amplitude in frequency domain and $PSD(u)$ and $R(u)$ are derive in equation(11)(18).

In order to align with the existing literature[32], $T = 1$ and $SNR = 1$, the sensitive form read as.

$$Sensitive(u) = \sqrt{PSD(u)/R(u)} \tag{22}$$

We show sensitivity curves for LISA, Taiji, and Tianqin detectors, and compare them with the most sensitive X configuration. Additionally, we compare the sensitivity of first-generation and second-generation optimal TDI for Taiji parameters. It is noteworthy that the X1 configura-

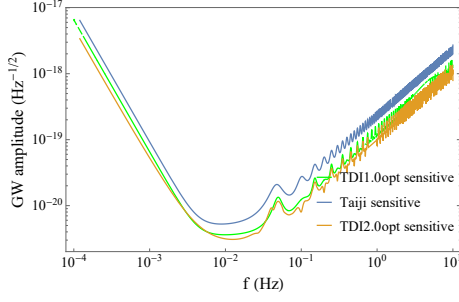


FIG. 8: TDI2.0opt is superior to the current best TDI1.0opt, which has a certain enhancement effect for the detection of dense binary wave source bands, while the effect is extremely significant for the SMBH wave source bands

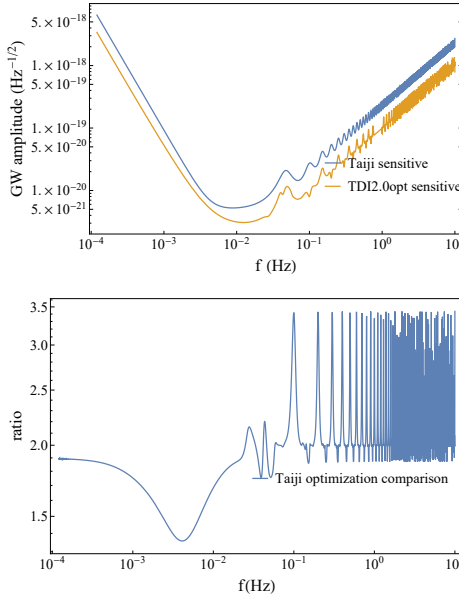


FIG. 9: The figure above shows the configuration sensitivity curves of TDI2.0opt and TDI1 with taiji parameter, and the figure below shows the relative optimization efficiency of TDI2.0opt

tion of the first-generation TDI has the same sensitivity as the X2 configuration of the second-generation TDI. (Figures 10, 9, 12, and 8).

D. Explore the factors influencing optimal TDI2.0

In this part, only three influential factors such as arm length, shot noise and accelerate noise were considered, and explore the change of sensitivity curve by change the parameter value.

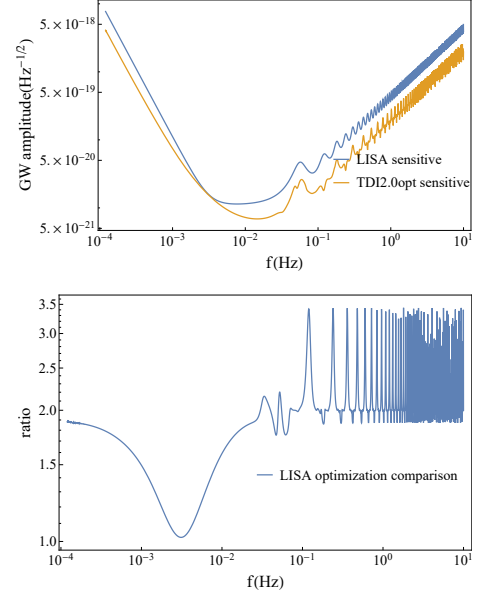


FIG. 10: The figure above shows the configuration sensitivity curves of TDI2.0opt and TDI1 with LISA parameter, and the figure below shows the relative optimization efficiency of TDI2.0opt

IV. SNR VALUES AND DETECTION RATES

A. Double White Dwarf

White dwarfs are highly compact objects located except to neutron stars and black holes. According to the existing cosmological and white dwarf formation models, it is estimated that there are about 10^9 double white dwarf systems [33]. Although there are many theoretical models of white dwarf formation mechanisms, such as CO+CO, CO+He, He+He, etc. [34], the evolution time of double white dwarfs is usually millions of years [35][36], which is far longer than the duration of current space-based gravitational wave observation missions. As a result, we can calculate the SNR value at a single frequency point, as the double white dwarfs evolve slowly in the frequency domain. The main consideration in this case is the detection rate of white dwarfs. For a continuous gravitational wave signal radiated by a compact double white dwarf system [35], its amplitude can be approximated as follows.

$$\begin{aligned}
 h(n, e) &= \left[\frac{16\pi G}{c^3 \omega_g^2} \frac{L(n, e)}{4\pi d^2} \right]^{1/2} \\
 &= 1.010^{-21} \frac{\sqrt{g(n, e)}}{n} \left(\frac{\mathcal{M}}{M_\odot} \right)^{5/3} \left(\frac{P_{\text{orb}}}{1\text{hr}} \right)^{-2/3} \left(\frac{d}{1\text{kpc}} \right)^{-1} \\
 g(n, e) &= \frac{1 + (73/24)e^2 + (37/96)e^4}{(1 - e^2)^{7/2}}
 \end{aligned} \tag{23}$$

If we don't think about the higher harmonic term and

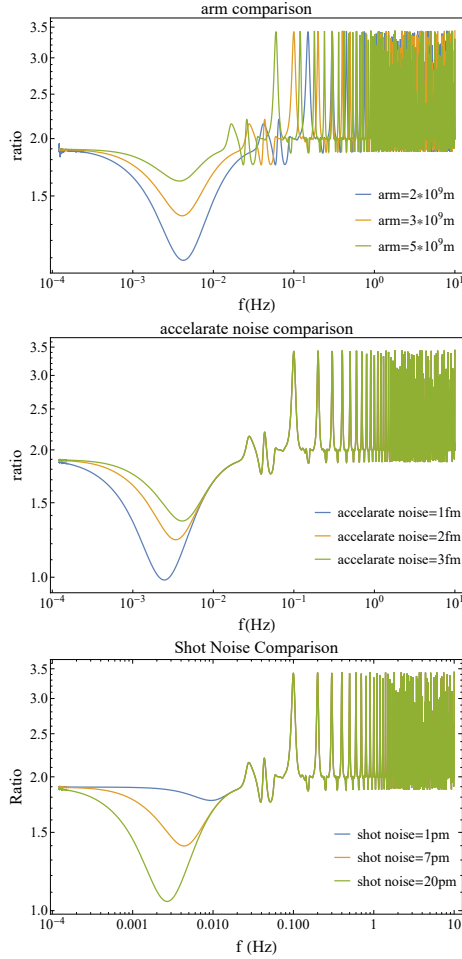


FIG. 11: The analysis focuses on taiji parameters, while other parameters yield similar results. Each comparison varies only the target parameter while keeping other parameters constant. The results indicate that the three factor parameters have no impact on high frequencies. In the low frequency region, arm length has a linear effect, with TDI2.0opt yielding better optimization with longer arm lengths. Shot noise suppression improves the optimization effect, while acceleration noise suppression reduces it.

choose Approximate circular orbit, $e=0, n=2$

$$h(0, 2) = 5.05 \times 10^{-22} \left(\frac{\mathcal{M}}{M_{\odot}} \right)^{5/3} \left(\frac{P_{orb}}{1hr} \right)^{-2/3} \left(\frac{d}{1kpc} \right)^{-1} \quad (24)$$

Introduce relation between f_{gw} and P_{orb} of DWD binary mass which mass is [24].

$$f_{gw} = \frac{2}{P_{orb}} = 2.3 \left(\frac{P_{orb}}{.01day} \right)^{-1} \text{ mHz} \quad (25)$$

substitute Equation (25) into Equation (24)

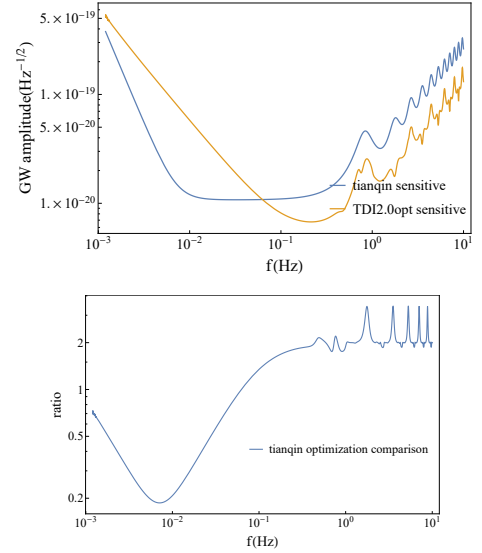


FIG. 12: The figure above shows the configuration sensitivity curves of TDI2.0opt and TDIX with tianqin parameter, and the figure below shows the relative optimization efficiency of TDI2.0opt

$$h(0, 2) = 5.05 \times 10^{-22} \left(\frac{\mathcal{M}}{M_{\odot}} \right)^{5/3} \left(\frac{(2.3 \cdot 10^{-3}/f_{gw}) \cdot 0.01 \cdot 24hr}{1hr} \right)^{-2/3} \left(\frac{d}{1kpc} \right)^{-1} \quad (26)$$

Taking into account the all sky average condition, And we get a concrete expression for SNR

$$SNR^2 = 5T \frac{(\frac{4}{5})^2 \tilde{h}(f)^2}{PSD(u)/R(u)} \quad (27)$$

Using the Taiji parameters, we calculate the all-sky average and verification sources of White Dwarf sources[33] for different TDI configurations using the above formula. The detailed results are shown in Appendix A. To explore the detection rate of White Dwarf sources ($SNR > 8$) under different TDI optimal, we randomly sample 1 million White Dwarf sources from the following parameter region using a random function.

$$\begin{aligned} m_1 &\sim [0.1, 1] M_{\odot} \\ m_2 &\sim [0.01, 0.1] M_{\odot} \\ D_{eff} &\sim [10, 50] Mpc \\ f &\sim [0.001, 0.01] Hz \end{aligned} \quad (28)$$

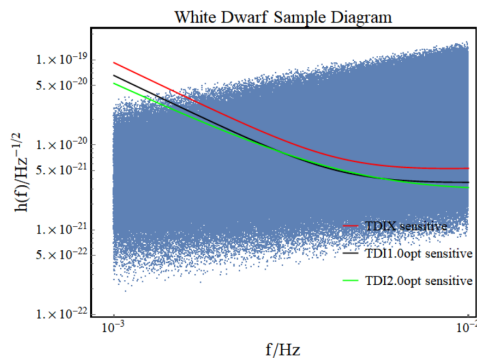


FIG. 13: One million samples of White Dwarf binaries (DWBS) were generated. With a threshold of $\text{SNR} > 8$, 53088 events were detected using TDIx, resulting in a detection rate of 5.30%. Similarly, 111950 events were detected using TDI1.0 optimal, resulting in a detection rate of 11.20%, while TDI2.0 optimal detected 130568 events with a detection rate of 13.05%.

During code calculate(Fig.13), The threshold is $\text{SNR} > 8$, TDIx get 53088 event and detection rate is 5.30%; TDI1.0 optimal get 111950 event and detection

rate is 11.20%; TDI2.0 optimal get 130568 event and detection rate is 13.05%.

V. CONCLUSION

In this study, we have presented the fundamental principles and applications of the second-generation optimal Time Delay Interferometry (TDI) technique. We began by providing a concise overview of the first-generation optimal TDI process, followed by an explanation of the conceptual foundation and development trajectory of the second-generation optimal TDI. Subsequently, we derived the power spectral density formula and sensitivity curve of the second-generation optimal TDI, comparing them to other TDI configurations. In the final section, we investigated the impact of various detector parameters on the optimization performance of TDI 2.0. Moreover, we assessed the signal-to-noise ratio and detection rate of White Dwarf systems based on the optimal TDI configuration. Based on this comprehensive analysis, we will consider different configuration effect on global fit problem and parameter estimate accuracy in future.

-
- [1] B. P. Abbott, R. Abbott, T. D. Abbott, M. R. Abernathy, F. Acernese, K. Ackley, C. Adams, and Adams, "Observation of gravitational waves from a binary black hole merger," *Phys. Rev. Lett.*, vol. 116, p. 061102, Feb 2016. [Online]. Available: <https://link.aps.org/doi/10.1103/PhysRevLett.116.061102> I
 - [2] B. P. Abbott, R. Abbott, T. D. Abbott, M. R. Abernathy, F. Acernese, and K. Ackley, "Observation of gravitational waves from a binary black hole merger," *Phys. Rev. Lett.*, vol. 116, p. 061102, Feb 2016. [Online]. Available: <https://link.aps.org/doi/10.1103/PhysRevLett.116.061102> I
 - [3] W. Chaibi, R. Geiger, B. Canuel, A. Bertoldi, A. Landragin, and P. Bouyer, "Low frequency gravitational wave detection with ground-based atom interferometer arrays," *Phys. Rev. D*, vol. 93, p. 021101, Jan 2016. [Online]. Available: <https://link.aps.org/doi/10.1103/PhysRevD.93.021101> I
 - [4] T. Accadia, F. Acernese, F. Antonucci, P. Astone, G. Ballardín, F. Barone, M. Barsuglia, A. Basti, T. S. Bauer, M. Bebronne, M. G. Beker, A. Belletoile, S. Birindelli, M. Bitossi, and M. A. Bizouard, "Status of the virgo project," *Classical and Quantum Gravity*, vol. 28, no. 11, p. 114002, may 2011. [Online]. Available: <https://dx.doi.org/10.1088/0264-9381/28/11/114002>
 - [5] G. M. Harry and (for the LIGO Scientific Collaboration), "Advanced ligo: the next generation of gravitational wave detectors," *Classical and Quantum Gravity*, vol. 27, no. 8, p. 084006, apr 2010. [Online]. Available: <https://dx.doi.org/10.1088/0264-9381/27/8/084006>
 - [6] B. P. Abbott, R. Abbott, R. Adhikari, P. Ajith, B. Allen, G. Allen, and R. S. Amin, "Ligo: the laser interferometer gravitational-wave observatory," *Reports on Progress in Physics*, vol. 72, no. 7, p. 076901, jun 2009. [Online]. Available: <https://dx.doi.org/10.1088/0034-4885/72/7/076901>
 - [7] S. Kawamura, M. Ando, N. Seto, S. Sato, T. Nakamura, and K. Tsubono, "The japanese space gravitational wave antenna: Decigo," *Classical and Quantum Gravity*, vol. 28, no. 9, p. 094011, apr 2011. [Online]. Available: <https://dx.doi.org/10.1088/0264-9381/28/9/094011> I
 - [8] K. Belczynski, M. Benacquista, and T. Bulik, "Double compact objects as low-frequency gravitational wave sources," *The Astrophysical Journal*, vol. 725, no. 1, p. 816, nov 2010. [Online]. Available: <https://dx.doi.org/10.1088/0004-637X/725/1/816> I
 - [9] C. Rodriguez, G. B. Taylor, R. T. Zavala, A. B. Peck, L. K. Pollack, and R. W. Romani, "A compact supermassive binary black hole system," *The Astrophysical Journal*, vol. 646, no. 1, p. 49, jul 2006. [Online]. Available: <https://dx.doi.org/10.1086/504825> I
 - [10] K. Danzmann and A. Rüdiger, "Lisa technology—concept, status, prospects," *Classical and Quantum Gravity*, vol. 20, no. 10, p. S1, apr 2003. [Online]. Available: <https://dx.doi.org/10.1088/0264-9381/20/10/301> I, III A
 - [11] W.-R. Hu and Y.-L. Wu, "The taiji program in space for gravitational wave physics and the nature of gravity," *National Science Review*, vol. 4, no. 5, pp. 685–686, 2017-10. [Online]. Available: <https://doi.org/10.1093/nsr/nwx116> I
 - [12] J. Luo, L.-S. Chen, H.-Z. Duan, Y.-G. Gong, S. Hu, J. Ji, Q. Liu, J. Mei, V. Milyukov, M. Sazhin, C.-G. Shao, V. T. Toth, H.-B. Tu, Y. Wang, Y. Wang, H.-C. Yeh, M.-S. Zhan, Y. Zhang, V. Zharov, and Z.-B. Zhou, "Tianqin: a space-borne gravitational wave detector," *Classical and Quantum Gravity*, vol. 33,

- no. 3, p. 035010, jan 2016. [Online]. Available: <https://dx.doi.org/10.1088/0264-9381/33/3/035010> I, III A
- [13] K. S. Thorne and C. J. Winstein, “Human gravity-gradient noise in interferometric gravitational-wave detectors,” *Phys. Rev. D*, vol. 60, p. 082001, Sep 1999. [Online]. Available: <https://link.aps.org/doi/10.1103/PhysRevD.60.082001> I
- [14] D. A. Shaddock, B. Ware, R. E. Spero, and M. Vallisneri, “Postprocessed time-delay interferometry for lisa,” *Phys. Rev. D*, vol. 70, p. 081101, Oct 2004. [Online]. Available: <https://link.aps.org/doi/10.1103/PhysRevD.70.081101> I
- [15] M. Otto, “Time-delay interferometry simulations for the laser interferometer space antenna,” *Ph.D. thesis, Gottfried Wilhelm Leibniz Universität Hannover*, Dec 2015. [Online]. Available: <https://doi.org/10.15488/8545> I
- [16] J. W. Armstrong, F. B. Estabrook, and M. Tinto, “Time-delay interferometry for space-based gravitational wave searches,” *The Astrophysical Journal*, vol. 527, no. 2, pp. 814–826, dec 1999. [Online]. Available: <https://doi.org/10.1086/2F308110>
- [17] P. Amaro-Seoane, H. Audley, S. Babak, and Baker. Laser interferometer space antenna. [Online]. Available: <http://arxiv.org/abs/1702.00786>
- [18] S. Babak, M. Hewitson, and A. Petiteau. Lisa sensitivity and snr calculations. [Online]. Available: <http://arxiv.org/abs/2108.01167>
- [19] M. Vallisneri, “Geometric time delay interferometry,” *Phys. Rev. D*, vol. 72, p. 042003, Aug 2005. [Online]. Available: <https://link.aps.org/doi/10.1103/PhysRevD.72.042003> I, II
- [20] M. Tinto and J. W. Armstrong, “Cancellation of laser noise in an unequal-arm interferometer detector of gravitational radiation,” *Phys. Rev. D*, vol. 59, p. 102003, Apr 1999. [Online]. Available: <https://link.aps.org/doi/10.1103/PhysRevD.59.102003> I
- [21] D. A. Shaddock, M. Tinto, F. B. Estabrook, and J. W. Armstrong, “Data combinations accounting for lisa spacecraft motion,” *Phys. Rev. D*, vol. 68, p. 061303, Sep 2003. [Online]. Available: <https://link.aps.org/doi/10.1103/PhysRevD.68.061303> I
- [22] K. R. Nayak, A. Pai, S. V. Dhurandhar, and J.-Y. Vinet, “Improving the sensitivity of lisa,” *Classical and Quantum Gravity*, vol. 20, no. 7, p. 1217, mar 2003. [Online]. Available: <https://dx.doi.org/10.1088/0264-9381/20/7/301> I
- [23] S. V. Dhurandhar, K. R. Nayak, and J.-Y. Vinet, “Algebraic approach to time-delay data analysis for lisa,” *Phys. Rev. D*, vol. 65, p. 102002, May 2002. [Online]. Available: <https://link.aps.org/doi/10.1103/PhysRevD.65.102002> I, II
- [24] K. R. Nayak, S. Dhurandhar, A. Pai, and J.-Y. Vinet, “Erratum: Optimizing the directional sensitivity of lisa [phys. rev. d 68, 122001 (2003)],” *Phys. Rev. D*, vol. 70, p. 049901, Aug 2004. [Online]. Available: <https://link.aps.org/doi/10.1103/PhysRevD.70.049901> I, IV A
- [25] K. R. Nayak, A. Pai, S. V. Dhurandhar, and J.-Y. Vinet, “Improving the sensitivity of lisa,” *Classical and Quantum Gravity*, vol. 20, no. 7, p. 1217, mar 2003. [Online]. Available: <https://dx.doi.org/10.1088/0264-9381/20/7/301> I, II
- [26] F. B. Estabrook, M. Tinto, and J. W. Armstrong, “Time-delay analysis of lisa gravitational wave data: Elimination of spacecraft motion effects,” *Phys. Rev. D*, vol. 62, p. 042002, Jul 2000. [Online]. Available: <https://link.aps.org/doi/10.1103/PhysRevD.62.042002> II
- [27] M. Tinto and S. Dhurandhar, “Time-delay interferometry,” *Living Reviews in Relativity*, vol. 17, 08 2014. [Online]. Available: <https://doi.org/10.12942/lrr-2014-6> II, II, II, II
- [28] P.-P. Wang, Y.-J. Tan, W.-L. Qian, and C.-G. Shao, “Sensitivity functions of space-borne gravitational wave detectors for arbitrary time-delay interferometry combinations regarding non-tensorial polarizations,” *Phys. Rev. D*, vol. 104, p. 023002, Jul 2021. [Online]. Available: <https://link.aps.org/doi/10.1103/PhysRevD.104.023002> II, III A, III B
- [29] M. Tinto, S. Dhurandhar, and D. Malakar, “Second-generation time-delay interferometry,” 2022. [Online]. Available: <https://doi.org/10.48550/arXiv.2212.05967> II
- [30] J. Sylvestre and M. Tinto, “Noise characterization for lisa,” *Phys. Rev. D*, vol. 68, p. 102002, Nov 2003. [Online]. Available: <https://link.aps.org/doi/10.1103/PhysRevD.68.102002> II
- [31] P.-P. Wang, W.-L. Qian, Y.-J. Tan, H.-Z. Wu, and C.-G. Shao, “Geometric approach for the modified second generation time delay interferometry,” *Phys. Rev. D*, vol. 106, p. 024003, Jul 2022. [Online]. Available: <https://link.aps.org/doi/10.1103/PhysRevD.106.024003> III A, III B
- [32] T. Robson, N. J. Cornish, and C. Liu, “The construction and use of lisa sensitivity curves,” *Classical and Quantum Gravity*, vol. 36, no. 10, p. 105011, apr 2019. [Online]. Available: <https://dx.doi.org/10.1088/1361-6382/ab1101> III C, III C
- [33] V. Korol, E. M. Rossi, P. J. Groot, G. Nelemans, S. Toonen, and A. G. A. Brown, “Prospects for detection of detached double white dwarf binaries with gaia, lsst and lisa,” *Monthly Notices of the Royal Astronomical Society*, vol. 470, no. 2, pp. 1894–1910, 2017. [Online]. Available: <https://doi.org/10.1093/mnras/stx1285> IV A, IV A
- [34] Korol, V., Toonen, S., Klein, A., Belokurov, V., Vincenzo, F., Buscicchio, R., Gerosa, D., Moore, C. J., Roebber, E., Rossi, E. M., and Vecchio, A., “Populations of double white dwarfs in milky way satellites and their detectability with lisa,” *A&A*, vol. 638, p. A153, 2020. [Online]. Available: <https://doi.org/10.1051/0004-6361/202037764> IV A
- [35] G. Nelemans, L. R. Yungelson, and S. F. P. Zwart, “The gravitational wave signal from the galactic disk population of binaries containing two compact objects,” *A&A*, vol. 375, no. 3, pp. 890–898, 2001-09-01. [Online]. Available: <https://www.aanda.org/articles/aa/abs/2001/33/aah2754/aah2754.html> IV A, IV A
- [36] H. Li, T. T. Zhang, T. Yilmaz, Y. Y. Pai, C. E. Marvinney, A. Said, Q. W. Yin, C. S. Gong, Z. J. Tu, E. Vescovo, C. S. Nelson, R. G. Moore, S. Murakami, H. C. Lei, H. N. Lee, B. J. Lawrie, and H. Miao, “Observation of unconventional charge density wave without acoustic phonon anomaly in kagome superconductors AV_3Sb_5 ($a = \text{Rb, Cs}$),” *Phys. Rev. X*, vol. 11, p. 031050, Sep 2021. [Online]. Available: <https://link.aps.org/doi/10.1103/PhysRevX.11.031050> IV A

VI. APPENDIX

A. Appendix A

TABLE II: SNR of verification WDB by different TDI optimal

source	m1	m2	D	f	TDIX	TDI1.0 opt	TDI2.0 opt
RX J0806	0.55	0.27	5000.0	6.22	73.20466546	103.2185783	106.9031338
V407 Vul	0.6	0.07	2000.0	3.51	23.35760705	32.93422594	32.06067987
ES Cet a	0.6	0.06	1000.0	3.22	33.47431685	47.19878676	46.58364111
AM CVn	0.71	0.13	600.0	1.94	38.19802502	53.85921527	59.84772028
SDSS J1908 +3940	0.6	0.05	1000.0	1.83	6.971176208	9.829358453	11.06409805
HP Lib	0.57	0.06	200.0	1.81	39.01688777	55.01381175	62.07102615
PTF1J1919+4815	0.6	0.04	2000.0	1.48	1.604789843	2.262753678	2.655675388
CR Boo	0.79	0.06	340.0	1.36	13.56142402	19.12160786	22.76736853
KL Dra	0.6	0.02	1000.0	1.33	1.222345144	1.723506653	2.059498637
V803 Cen	0.84	0.08	350.0	1.25	14.54524331	20.50879307	24.74228728
SDSS J0926a	0.85	0.04	460.0	1.18	4.858215239	6.850083488	8.333222696
CP Eri	0.6	0.02	700.0	1.18	1.27107637	1.792217682	2.180257962
2003aw	0.6	0.02	700.0	0.99	0.796850852	1.123559701	1.397711946
2QZ 1427 -01	0.6	0.015	700.0	0.91	0.478818637	0.675134277	0.847658674
SDSS J1240	0.6	0.01	400.0	0.89	0.527949775	0.744409182	0.936774109
SDSS J0804	0.6	0.01	400.0	0.75	0.334608933	0.471798595	0.603077458
SDSS J1411	0.6	0.01	400.0	0.72	0.300111961	0.423157865	0.542663268
GP Com	0.6	0.01	80.0	0.72	1.500559803	2.115789323	2.713316342
SDSS J0902	0.6	0.01	500.0	0.69	0.214340172	0.302219643	0.388814525
SDSS J1552	0.6	0.01	500.0	0.59	0.14119636	0.199086868	0.25877857
CE 315	0.6	0.006	77.0	0.51	0.373830458	0.527100945	0.690411278
J0651+2844	0.55	0.25	1000.0	2.61	73.4804528	103.6074384	107.1526116
J0935+4411	0.32	0.14	660.0	1.68	14.15056171	19.95229201	22.86245848
J0106-1000	0.43	0.17	2400.0	0.85	0.953669274	1.344673677	1.699849017
J1630+ 4233	0.31	0.52	830.0	0.84	5.288218978	7.456388759	9.436507768
J1053+ 5200	0.2	0.26	1100.0	0.54	0.482579313	0.680436831	0.888758012
J0923+ 3028	0.279	0.37	228.0	0.51	3.538424739	4.989178882	6.534963372
J1436 + 50107	0.24	0.46	800.0	0.51	1.051639414	1.482811574	1.942227278
WD 0957-666	0.32	0.37	135.0	0.38	3.064335551	4.320713126	5.721886223
J0755+ 4906	0.176	0.81	2620.0	0.37	0.157200549	0.221652774	0.293754057
J0849+ 0445	0.176	0.65	1004.0	0.29	0.182363771	0.257132917	0.342640677
J0022-1014	0.21	0.375	1151.0	0.29	0.122846528	0.173213604	0.230814581
J2119-0018	0.74	0.158	2610.0	0.27	0.057628499	0.081256184	0.108406889
J1234-0228	0.09	0.23	716.0	0.25	0.042725893	0.060243509	0.080463381
WD 1101+ 364	0.36	0.31	97.0	0.16	0.404291575	0.570051121	0.7644969
WD 0931+4445	0.32	0.14	660.0	1.67	13.93049078	19.64199201	22.53379912
WD 1242-105	0.56	0.39	39.0	0.19	2.76990409	3.905564767	5.231591232
J0056-0611	0.174	0.46	585.0	0.53	1.194042867	1.683600443	2.201126945
J0106- 1000	0.191	0.39	2691.0	0.85	0.876060914	1.235245889	1.561517523
J0345+1748d	0.76	0.181	166.0	0.1	0.074249388	0.104691638	0.140651886
J0745+ 1949d	0.1	0.156	270.0	0.21	0.05777962	0.081469264	0.109032903
J0751-0141	0.97	0.194	1859.0	0.29	0.144504936	0.20375196	0.271508255
J0825+ 1152d	0.49	0.287	1769.0	0.4	0.306112419	0.431618511	0.570704449
J1053+5200	0.26	0.213	1204.0	0.54	0.465211102	0.655947654	0.856771277
J1054-2121	0.39	0.168	751.0	0.22	0.076177336	0.107410044	0.143682038
.J1056+ 6536	0.34	0.338	1421.0	0.53	0.690171093	0.973141241	1.272277765
.J1108+ 1512	0.42	0.167	698.0	0.19	0.058355556	0.082281334	0.110217685
J1112+1117	0.14	0.169	257.0	0.13	0.024068587	0.033936708	0.045557547
J1130+ 3855	0.72	0.286	662.0	0.15	0.080363363	0.113312341	0.152016741
J1436+ 5010	0.46	0.233	830.0	0.51	0.987366444	1.392186686	1.823524315
J1443+ 1509	0.84	0.181	540.0	0.12	0.039921919	0.056289906	0.075586649
J1630+ 4233	0.3	0.307	820.0	0.84	3.394413377	4.786122861	6.057125911
J1741 + 6526	1.11	0.17	936.0	0.38	0.573272106	0.80831367	1.070443401
J1840+ 6423	0.65	0.177	676.0	0.12	0.025887731	0.0365017	0.049014848
J2338-2052	0.15	0.263	1295.0	0.3	0.067240209	0.094808695	0.126257818
CSS 41177	0.36	0.31	473.0	0.24	0.244447101	0.344670412	0.460599618
J1152 +0248	0.47	0.41	464.0	0.23	0.350741252	0.494545166	0.661224238